

Flow-based generative models as iterative algorithms in probability space

Yao Xie* Xiuyuan Cheng[†]

Abstract

Generative AI (GenAI) has revolutionized data-driven modeling by enabling the synthesis of high-dimensional data across various applications, including image generation, language modeling, biomedical signal processing, and anomaly detection. Flow-based generative models provide a powerful framework for capturing complex probability distributions, offering exact likelihood estimation, efficient sampling, and deterministic transformations between distributions. These models leverage invertible mappings governed by Ordinary Differential Equations (ODEs), enabling precise density estimation and likelihood evaluation. This tutorial presents an intuitive mathematical framework for flow-based generative models, formulating them as neural network-based representations of continuous probability densities. We explore key theoretical principles, including the Wasserstein metric, gradient flows, and density evolution governed by ODEs, to establish convergence guarantees and bridge empirical advancements with theoretical insights. By providing a rigorous, yet accessible treatment, we aim to equip researchers and practitioners with the necessary tools to effectively apply flow-based generative models in signal processing and machine learning.

1 Introduction

Generative AI (GenAI) has revolutionized data-driven modeling by enabling the synthesis of high-dimensional data in fields such as image generation, large language models (LLMs), biomedical signal processing, and anomaly detection. Among GenAI approaches, diffusion-based (see, e.g., [33, 17, 34]) and flow-based [20, 10, 11, 19, 14, 6, 24, 1, 25, 38] generative models have gained prominence due to their ability to model complex distributions sample generation and density estimation.

Flow-based models leverage invertible mappings governed by Ordinary Differential Equations (ODEs), unlike diffusion models, which rely on iterative denoising through Stochastic Differential Equations (SDEs). The design of flow-based models provides a direct and deterministic transformation between probability distributions, enabling exact likelihood estimation and fast sampling.

*H. Milton Stewart School of Industrial and Systems Engineering, Georgia Institute of Technology. Email: yao.c.xie@gmail.com.

[†]Department of Mathematics, Duke University. Email: xiuyuan.cheng@duke.edu

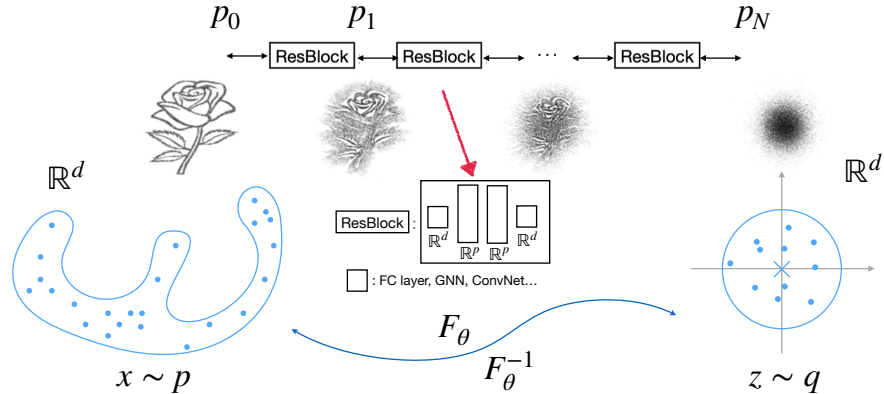


Figure 1: General setup of a flow-based generative model, where the forward process is captured through a forward mapping F_θ , and the reverse process is captured by the inverse mapping F_θ^{-1} . Arrows indicate the forward-time flow from the data distribution p to the target distribution q (typically Gaussian noise). The forward process maps p to the noise distribution q , while the reverse process reconstructs p from q . Both processes involve a sequence of transported densities at discrete time steps, with ResNet blocks serving as iterative steps that push densities in probability space under the Wasserstein-2 metric.

This makes them particularly well-suited for tasks requiring density estimation and likelihood evaluation, such as anomaly detection and probabilistic inference. While empirical advancements in generative models have been substantial, a deeper understanding of the design and mathematical foundations of flow-based generative models will enable both theoreticians and practitioners to broaden their adoption for diverse applications in signal processing and leverage them as a general representation of high-dimensional distributions.

This tutorial presents an intuitive mathematical framework for flow-based generative models, viewing them as neural network-based representations of continuous probability densities. These models can be cast as particle-based iterative algorithms in probability space using the Wasserstein metric, providing both theoretical guarantees and computational efficiency. Based on this framework, we establish the convergence of the iterative algorithm and show the generative guarantee, ensuring that under suitable conditions, the learned density approximates the true distribution. By systematically building from fundamental concepts to state-of-the-art research, our goal is to guide the audience from a basic understanding to the research frontiers of generative modeling, demonstrating its impact on signal processing, machine learning, and beyond.

2 Mathematical background

In this section, we introduce the essential mathematical background for understanding flow-based generative models. We start with the concept of an ODE and the *velocity field*, which describe the continuous transformations applied to data samples (particles) as they progress through the model. Following this, we examine how data density evolves using the *continuity equation*, which

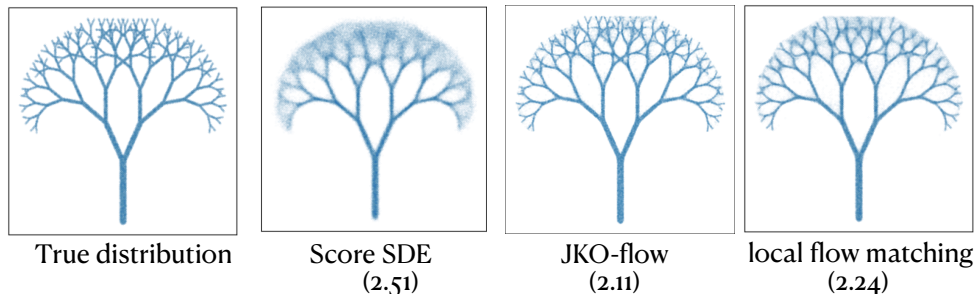


Figure 2: Illustrative example of generating a two-dimensional “fractal tree” distribution using various flow-based generative models. The numbers in brackets represent the negative log-likelihood (NLL), where lower values indicate better performance. Note that the flow-based generative model captures finer details of the distribution more effectively, while JKO-flow [38] achieves a lower (better) NLL score, at the cost of higher computational cost than local Flow Matching [39].

characterizes changes in probability density over time within the transformation. We then introduce the SDE and the associated Fokker-Planck equation (FPE), and explain its relationship to the continuity equation. Finally, we provide the preliminaries of Wasserstein space and the Optimal Transport map.

2.1 ODE and Continuity Equation

Consider a space where the data (particle) $x(t) \in \mathbb{R}^d$ lies in; we describe the dynamic of the data using an ODE

$$\dot{x}(t) = v(x(t), t), \quad t \in [0, T], \quad (1)$$

where $\dot{x}(t) = \frac{d}{dt}x(t)$, $v(x, t) : \mathbb{R}^d \rightarrow \mathbb{R}^d$ is call the *velocity field*, which describes how the a particle evolves; the velocity field can vary over the position x and time t . We also write $v(\cdot, t) = v_t(\cdot)$. As the participle evolves according to the dynamic, its underlying distribution also evolves over time, which is governed by the *continuity equation* (CE), also known as *Liouville equation*). Taking the continuous-time formulation (1), let P be the data distribution with density p , $x(0) \sim p$, and denote by $\rho_t(x) = \rho(x, t)$ the probability density of $x(t)$. Then ρ_t solve the CE as

$$\partial_t \rho_t + \nabla \cdot (\rho_t v_t) = 0, \quad (2)$$

from $\rho_0 = p$. Here the divergence operator follows the standard definition in vector calculus: for a vector field $u(x) = [u_1(x), \dots, u_d(x)]$ for $x \in \mathbb{R}^d$, $\nabla \cdot u(x) = \sum_{j=1}^d \partial u_j(x) / \partial x_j$.

Mathematically, the solution trajectory of ODE is well-defined: given the initial value problem, ODE is well-posed under certain regularity conditions of the velocity field v , meaning that the ODE solution exists, is unique, and continuously depends on the initial value. Informally, the CE (2) provides insights of how data distribution changes from a simple initial state into a more complex target distribution: If the algorithm can find a v_t such that ρ_T at some time T is close to q , then one would expect the reverse-time flow from $t = T$ to $t = 0$ to transport from q to a distribution

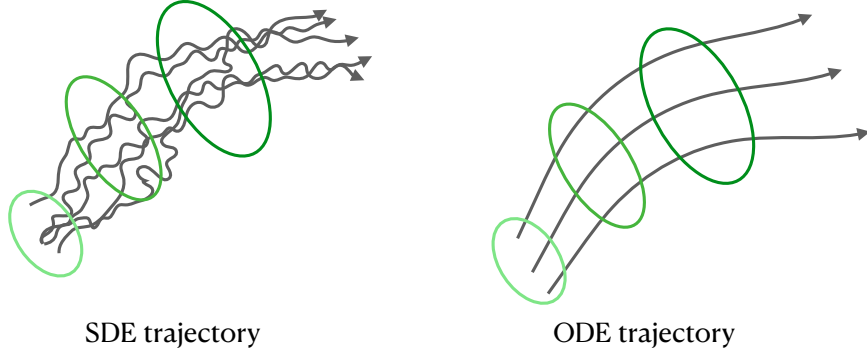


Figure 3: Trajectory of SDE versus ODE: The SDE trajectory corresponds to a diffusion model, while for ODE, the dynamics are deterministic, but the initial position of the trajectory follows a distribution.

close to p . Normalizing flow models drive data distribution towards a target distribution q typically normal, $q = \mathcal{N}(0, I_d)$, per the name “normalizing.”

2.2 SDE and Fokker-Plank Equation

Another popular type of generative model, namely the Diffusion Models, is based on the following SDE (under a change of time reparametrization, see, e.g. [8]):

$$dX_t = -X_t dt + \sqrt{2} dW_t, \quad (3)$$

which is known as the Ornstein-Uhlenbeck (OU) process in \mathbb{R}^d , and dW_t denotes the standard Brownian motion. More generally, one can consider a diffusion process

$$dX_t = -\nabla V(X_t) dt + \sqrt{2} dW_t, \quad X_0 \sim P. \quad (4)$$

Here, the ∇f finds the gradient of a scalar function $f : \mathbb{R}^d \rightarrow \mathbb{R}$, and the OU process is a special case with $V(x) = \|x\|^2/2$. We denote by ρ_t the marginal distribution of X_t for $t > 0$. The time evolution of ρ_t is described by the FPE written as

$$\partial_t \rho_t = \nabla \cdot (\rho_t \nabla V + \nabla \rho_t). \quad (5)$$

Note that the density evolution through the CE (2) and the FPE (5) are mathematically equivalent when we set

$$v(x, t) = -\nabla V(x) - \nabla \log \rho(x, t). \quad (6)$$

However, these two approaches lead to very different trajectories (as illustrated in Fig. 3) and algorithms: the flow-based model learns the velocity field v , which is implicitly related to the score function $\nabla \log \rho$ that the diffusion generative model learns in the forward process and uses in the reverse-time generative process, illustrated in Fig. 1.

2.3 Wasserstein space and Optimal Transport

We also review the definitions of the Wasserstein-2 distance and optimal transport (OT) map, which are connected by the Brenier Theorem (see, e.g., [3, Section 6.2.3]). Denote by \mathcal{P}_2 the space of probability distributions on \mathbb{R}^2 with finite second moments, namely $\mathcal{P}_2 = \{P \text{ on } \mathbb{R}^d, \text{ s.t.}, \int_{\mathbb{R}^d} \|x\|^2 dP(x) < \infty\}$, and denote by \mathcal{P}_2^r the distributions in \mathcal{P}_2 that have densities. Given two distributions $\mu, \nu \in \mathcal{P}_2$, the Wasserstein-2 distance $\mathcal{W}_2(\mu, \nu)$ is defined as

$$\mathcal{W}_2^2(\mu, \nu) := \inf_{\pi \in \Pi(\mu, \nu)} \int_{\mathbb{R}^d \times \mathbb{R}^d} \|x - y\|^2 d\pi(x, y), \quad (7)$$

where $\Pi(\mu, \nu)$ denotes the family of all joint distributions with μ and ν as marginal distributions. When P and Q are in \mathcal{P}_2^r and have densities p and q respectively, we also denote $\mathcal{W}_2(P, Q)$ as $\mathcal{W}_2(p, q)$. When at least μ has density, we have the following result by the Brenier Theorem, which allows us to define the optimal transport (OT) map: The unique minimizer of (7) is achieved at $\pi = (\text{Id}, T_\mu^\nu)_\# \mu$, where Id denotes the identity map, T_μ^ν is the OT map from μ to ν which is μ -a.e. defined. Here, the *pushforward* of a distribution P , by a map $F : \mathbb{R}^d \rightarrow \mathbb{R}^d$, is denoted as $F_\# P$, such that $F_\# P(A) = P(F^{-1}(A))$ for any measurable set A in \mathbb{R}^d . The minimum of (7) also equals that of the Monge problem, namely

$$\mathcal{W}_2^2(\mu, \nu) = \inf_{F: \mathbb{R}^d \rightarrow \mathbb{R}^d, F_\# \mu = \nu} \int \|x - F(x)\|^2 d\mu(x). \quad (8)$$

3 Algorithm basics of generative flow models

Normalizing Flow (NF) is a class of deep generative models for efficient sampling and density estimation. Compared to diffusion models, NF models [20] appear earlier in the generative model literature. Fig. 1 illustrates the general setup of flow-based generative models.

To be more specific, NFs are transformations that map an easy-to-sample initial distribution, such as a Gaussian, to a more complex target distribution. Generally, an NF model provides an invertible *flow mapping* $F_\theta : \mathbb{R}^d \rightarrow \mathbb{R}^d$, parametrized by θ (usually a neural network), such that it maps from the “code” or “noise” z (typically Gaussian distributed) to the data sample $x \sim p$, where p is the unknown underlying data distributions. We are only given the samples from the data distribution p as training data. Once a flow model F_θ is trained, one can generate samples x by computing $x = F_\theta(z)$ and drawing $z \sim q$, where q is a distribution convenient to sampling in high dimensional, typically $q = \mathcal{N}(0, I)$.

3.1 Training objective and particle-based implementation

NFs aim to learn the transform from a simple distribution to a complex data distribution by maximizing the log-likelihood of the observed data. In terms of algorithm, the training aims to find the flow map F_θ that minimizes the training objective.

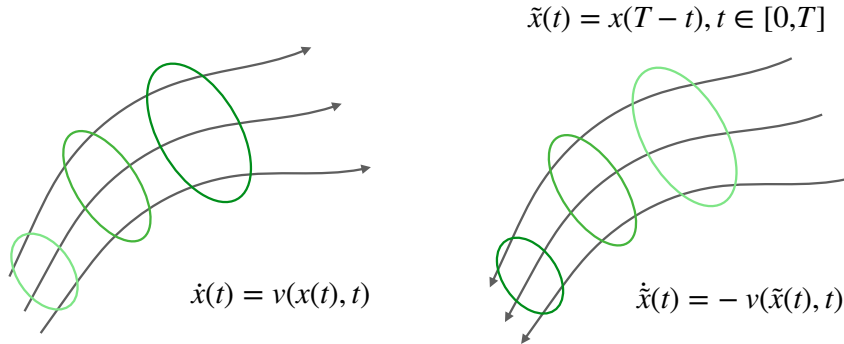


Figure 4: Reverse time dynamic of ODE: ODE can go forward or backward in time deterministically.

Given a dataset $\{x^i\}_{i=1}^m$ (referred to as “particles”), we assume that each x^i is sampled from an unknown distribution p , and want to approximate it with our flow model $p_\theta(x)$. The model transforms a simple target distribution q , e.g., $\mathcal{N}(0, I)$, into p_θ using the invertible mapping F_θ . The log-likelihood of a data point x under the flow model F_θ is then

$$\log p_\theta(x) = \log p_z(F_\theta^{-1}(x)) + \log \left| \det J_{F_\theta^{-1}}(x) \right|, \quad (9)$$

where $p_z(z)$ is the density of the noise (Gaussian distribution), F_θ^{-1} maps the data x back to the noise space, and $\det J_{F_\theta^{-1}}(x)$ is the Jacobian determinant of the inverse transformation, capturing how the transformation scales probability mass. To train the model, maximizing the total log-likelihood over all training samples leads to minimizing the negative log-likelihood (NLL):

$$\mathcal{L}(\theta) = -\frac{1}{m} \sum_{i=1}^m \left[\log p_z(F_\theta^{-1}(x^i)) + \log \left| \det J_{F_\theta^{-1}}(x^i) \right| \right], \quad (10)$$

which serves as a training objective.

Since NFs are differentiable, $\mathcal{L}(\theta)$ can be optimized using stochastic gradient descent (SGD) or variants such as Adam. The gradient of the loss function can be computed using backpropagation through the invertible transformations. However, depending on the way of parameterizing F_θ , the computation of likelihood and backpropagation training can be expensive and challenging to scale to high dimensional data. The key to design a flow model is to construct F_θ for efficient training and generation, which we detail in below.

3.2 Discrete-time Normalizing Flow

Largely speaking, NFs fall into two categories: discrete-time and continuous-time. The discrete-time NF models typically follow the structure of a Residual Network (ResNet) [16] and consist of a sequence of mappings:

$$x_n = x_{n-1} + f_n(x_{n-1}), \quad n = 1, \dots, N, \quad (11)$$

where each f_n is a neural network mapping parameterized by the n -th ‘‘Residual Block’’, and x_n is the output of the n -th block. The composition of the N mappings $x_{n-1} \mapsto x_n$, $n = 1, \dots, N$, together provides the (inverse of the) flow mapping F_θ , the invertibility of which needs to be ensured by additional techniques and usually by enforcing each block mapping $x_{n-1} \mapsto x_n$ to be invertible. The computation of the inverse mapping, however, may not be direct. After training, the generation of x is by sampling $z \sim q$ and computing $z \mapsto x$ is via the flow map computed through N blocks.

Meanwhile, for the discrete-time flow (11), the computation of the likelihood (9) calls for the computation of the log-determinant of the Jacobian of f_n . This can be challenging for a general multivariate mapping f_n . To facilitate these computations, earlier NFs such as NICE [10], Real NVP [11], and Glow [19] adopted special designs of the neural network layer type in f_n in each block. While the special designs improve the computational efficiency of invertibility and log determinant of Jacobian, it usually restrict the expressiveness of the Residual block and consequently the accuracy of the NF model.

3.3 Continuous-time Normalizing Flow based on neural ODE

Continuous-time NFs [14] are implemented under the neural ODE framework [6], where the neural network features $x(t)$ is computed by integrating an ODE as introduced in (1), and $v(x, t)$ is parametrized by a neural ODE network. We use v_θ to denote the parameterization. A notable advantage of the continuous-time NF is that the neural ODE framework allows to compute the forward/inverse flow mapping as well as the likelihood by numerical integration.

- Forward/inverse flow mapping:

In the continuous-time flow, invertibility is presumed since a well-posed (neural) ODE can be integrated in two directions of time alike, as illustrated in Fig. 4. Specifically, let $x(t)$ be the ODE solution trajectory satisfying $\dot{x}(t) = v_\theta(x(t), t)$ on $[0, T]$, the flow mapping can be written as

$$F_\theta(x) = x + \int_0^T v_\theta(x(t), t) dt, \quad x(0) = x, \quad (12)$$

The inverse mapping F_θ^{-1} can be computed by integrating reverse in time. In actual implementation, these integrals are calculated on a discrete time grid on $[0, T]$ using standard numerical integration schemes [6].

- Likelihood by instantaneous change-of-variable:

For flow trajectory $x(t)$ satisfying (1), suppose $x(0)$ has a distribution $x(0) \sim p = p_0$ and this induces the marginal density p_t of $x(t)$. The so-called instantaneous change-of-variable formula [14] gives the relation

$$\log p_t(x(t)) - \log p_s(x(s)) = - \int_s^t \nabla \cdot v_\theta(x(\tau), \tau) d\tau, \quad (13)$$

which involves the time-integration of the trace of the Jacobian of v_θ . In practice, the divergence term averaged over samples is often estimated by the Hutchinson approximation. While these computations may still encounter challenges in high dimensions, the ability to evaluate the (log) likelihood is fundamentally useful; in particular, it allows for evaluating the maximum likelihood training objective on finite samples. This property is also adopted in the deterministic reverse process in diffusion models [33], called the “probability flow ODE”, so the likelihood can be evaluated once a forward diffusion model has been trained.

Because the invertibility and likelihood computation is guaranteed by the continuous-time formulation, there is no need to design special architecture in the neural network parametrization of v_θ , which makes the continuous-time NF “free-form” [14]. This allows to leverage the full expressive power of deep neural network layers as well as problem-specific layer types in each Residual block f_n depending on the application at hand. For example, in addition to the basic feed-forward neural networks, one can use convolutional neural networks (CNN) if the data are images, and graph neural networks (GNN) to generate data on graphs.

3.4 Discrete-time flow as iterative steps

We first would like to point out that the distinction between discrete-time versus continuous-time flow models is not strict since continuous-time flow needs to be computed on a discrete time grid in practice – recalling that the ResNet block (11) itself can be viewed as a Forward Euler scheme to integrate an ODE. In particular, one can utilize the benefit of continuous-time NF (neural ODE) inside the discrete-time NF framework by setting the n -th block f_n to be a neural ODE on a subinterval of time.

Specifically, let the time horizon $[0, T]$ be discretized into N subintervals $[t_{n-1}, t_n]$ and $x(t)$ solves the ODE with respect to the velocity field $v_\theta(x, t)$. The n -th block mapping (associated with the subinterval $[t_{n-1}, t_n]$) is defined as

$$x_n = x_{n-1} + \int_{t_{n-1}}^{t_n} v_\theta(x(t), t) dt, \quad x(t_{n-1}) = x_{n-1}. \quad (14)$$

This allows the computation of the likelihood via integrating ∇v_θ by (13) (and concatenating the N subintervals), and the inverse mapping $x_n \mapsto x_{n-1}$ of each block again can be computed by integrating the ODE reverse in time.

In short, by adopting a continuous-time NF sub-network inside each Residual block, one can design a discrete-time flow model that is free-form, automatically invertible (by using small enough time step to ensure sufficiently accurate numerical integration of the ODE such that the ODE trajectories are distinct), and enjoys the same computational and expressive advantage as continuous-time NF. One subtlety, however, lies in the parametrization of v_θ : in the standard continuous-time NF, $v_\theta(x, t)$ is “one-piece” from time 0 to T , while when putting on a discrete time grid with N time stamps, $v_\theta(x, t)$ on the subinterval $[t_{n-1}, t_n]$ provides the parametrization of f_n in (11) and can be

parametrized independently from the other blocks (as is usually done in ResNet).

If using independent parametrization of v_θ on $[t_n, t_{n-1}]$, the n -th block can potentially be trained independently and *progressively* – meaning that only one block is trained at a time and the n -th block is trained only after the previous $(n - 1)$ blocks are fully trained and fixed (see Figure 5) – but the training objective needs to be modified from the end-to-end likelihood (9). Such training of flow models in a progressive manner has been implemented under various context in literature, particularly in [2, 27, 13, 38, 35] motivated by the Jordan-Kinderlehrer-Otto (JKO) scheme, which we will detail more in Section 4. The progressive training intuitively enables incremental evolution of probability distributions over time. Experimentally, it has been shown to improve the efficiency of flow-based generative models (by reducing computational and memory load in training each block) while maintaining high-quality sample generation. From a theoretical point of view, the discrete-time Residual blocks in such flow models can naturally be interpreted as “steps” in certain iterative Gradient Descent scheme that minimizes a variational objective over the space of probability densities.

3.5 Simulation-free training: Flow Matching

While continuous-time NFs enjoy certain advantages thanks to the neural ODE formulation, a computational bottleneck for high dimensional data is the computation of $\nabla \cdot v_\theta$ in (13). The back-propagation training still needs to track the gradient field along the numerical solution trajectories of the neural ODE, which makes the approach “simulation-dependent” and computationally costly. In contrast, the recent trend in deep generative models focuses on “simulation-free” approaches, where the training objective is typically an L^2 loss (mean squared error) that “matches” the neural network velocity field $v_\theta(x, t)$ to certain target ones. Such simulation-free training has been achieved by Diffusion Models [17, 34] as well as Flow Matching (FM) models [24, 1, 25]. FM ensures that the learned velocity field satisfies CE, is computationally efficient, and potentially enables efficient sample generation with fewer steps. FM models have demonstrated state-of-the-art performance across various applications, such as text-to-image generation [12], humanoid robot control [31], and audio generation [15].

Here we provide a brief review of the latter, primarily following the formulation in [1]. The FM model still adopts continuous-time neural ODE and the time interval is $[0, 1]$. FM utilizes a pre-specified “interpolation function” I_t , parametrized by $t \in [0, 1]$, which smoothly connects samples for two endpoints x_0 and x_1 defined as

$$\phi(t) := I_t(x_0, x_1), \quad t \in [0, 1], \tag{15}$$

where $x_0 \sim p$, $x_1 \sim q$. Common interpolation function is a straight line from x_0 to x_1 . The model is trained to match the velocity field $v_\theta(x, t)$, denoted as \hat{v} here, to the true probability flow induced

by I_t via minimizing the (population) loss

$$L(\hat{v}) := \int_0^1 \mathbb{E}_{x_0, x_1} \left\| \hat{v}(\phi(t), t) - \frac{d}{dt} \phi(t) \right\|^2 dt. \quad (16)$$

Here we suppress the parameter θ in notation as we assume sufficient expressiveness of the flow network and for simplicity consider the unconstrained minimization of the field $\hat{v}(x, t)$.

While not immediate from its appearance, the minimization of (16) gives a desired velocity field that leads us to the correct target. Formally, we call a velocity field $v(x, t)$ on $\mathbb{R}^d \times [0, 1]$ “valid” if it provides a desired transport from p to q , i.e., the continuity equation (CE) $\partial_t \rho + \nabla \cdot (\rho v) = 0$ starting from $\rho(\cdot, 0) = p$ satisfies $\rho(\cdot, 1) = q$. It can be shown that there is a valid v (depending on the choice of I_t) such that, up to a constant, $L(\hat{v})$ is equivalent to the L^2 loss $\int_0^1 \int_{\mathbb{R}^d} \|\hat{v}(x, t) - v(x, t)\|^2 \rho_t(x) dx dt$ where ρ_t solves the CE induced by v . This has been derived in [1]; here we include the argument (allowing x_0 and x_1 to be dependent) in the following lemma for completeness (proof in appendix).

Lemma 3.1 (Consistency of FM loss). *Given p, q and the interpolation function I_t , there exists a valid velocity field v such that, with $\rho_t(x) = \rho(x, t)$ being the solution of the induced CE by v , the loss $L(\hat{v})$ can be written as*

$$L(\hat{v}) = c + \int_0^1 \int_{\mathbb{R}^d} \|\hat{v}(x, t) - v(x, t)\|^2 \rho_t(x) dx dt, \quad (17)$$

where c is a constant independent from \hat{v} .

A direct result of the lemma is that the (unconstrained) minimizer of the MF loss (16) is $\hat{v} = v$ and it is a valid velocity field. In practice, the training of $\min L(\hat{v})$ from finite samples is via the empirical version of (16).

4 Flow as iterative algorithm in probability space

In this section, we elaborate on flow models that implement iterative steps to minimize a variational objective in the Wasserstein space. We will detail on the flow motivated by the JKO scheme and the theoretical analysis of the generation accuracy.

4.1 Iterative flow using JKO scheme

We consider discrete-time flow models where each block can potentially take form of a continuous-time NF (neural ODE), following the set up in Section 3.4. As has been shown in Section 3, in the (end-to-end) training of a flow model all the N blocks (or the entire flow on $[0, T]$) are optimized simultaneously using a single objective, usually the max-likelihood. In contrast, the progressive training will train each block sequentially and independently, attaching a loss specific to the block during training, see Figure 5. We call such flow implementing the iterative steps the *iterative flow*, and the key is to design a step-wise loss to train each block.

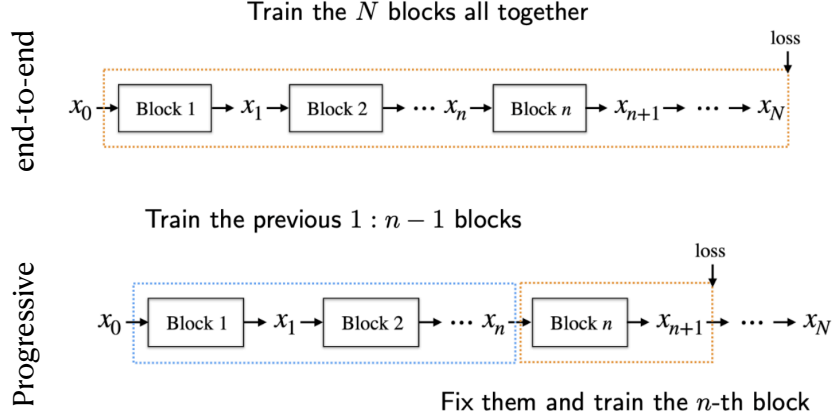


Figure 5: End-to-end versus progressive training of a flow model consisting of N Residual blocks.

For iterative flow models motivated by the JKO scheme (here our presentation illustrates the framework from [38, 8]), the step-wise loss is the Kullback-Leibler (KL) divergence to the known target distribution $q \propto e^{-V}$, namely

$$\text{KL}(\rho||q) = \int \rho(x) \log \rho(x) dx + \int V(x) \rho(x) dx + \text{const.} \quad (18)$$

Specifically, the classical JKO scheme [18] computes a sequence of distributions ρ_n , $n = 0, 1, \dots$ by

$$\rho_{n+1} = \arg \min_{\rho \in \mathcal{P}_2} \text{KL}(\rho||q) + \frac{1}{2\gamma} \mathcal{W}_2^2(\rho_n, \rho), \quad (19)$$

starting from $\rho_0 \in \mathcal{P}_2$, where $\gamma > 0$ controls the step size. In the context of normalizing flow, the sequence starts from $\rho_0 = p$ the data density and the density ρ_n evolves to approach q as n increases.

Strictly speaking, the minimization in (19) is over the Wasserstein-2 space of the density ρ , which, in the n -th JKO flow block will apply to the pushforwarded density by the mapping in the n -th block. In other words, define the forward mapping (14) in the n -th block as F_n , i.e. $x_n = F_n(x_{n-1})$, and in view of (11), $F_n(x) = x + f_n(x)$; The parametrization of F_n is via $v_\theta(x, t)$ on $t \in [t_{n-1}, t_n]$, so we write $F_{n,\theta}$ to emphasize the parametrization. We denote by p_n the marginal distribution of x_n , where $p_0 = p$ (x_0 follows the data distribution), and then we have

$$p_n = (F_{n,\theta})_{\#} p_{n-1}. \quad (20)$$

Following (19), the training of the n -th JKO flow block is by

$$\min_{\theta} \text{KL}((F_{n,\theta})_{\#} p_{n-1} || q) + \frac{1}{2\gamma} \mathcal{W}_2^2(p_{n-1}, (F_{n,\theta})_{\#} p_{n-1}), \quad (21)$$

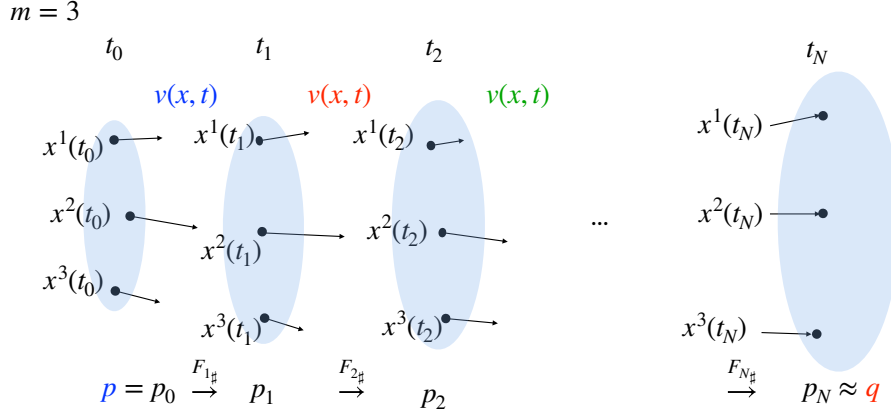


Figure 6: Example of JKO flow scheme based on particle implementation, see more in Section 4.1.

which is equivalent to the following objective [38]

$$\min_{\theta} \text{KL}((F_{n,\theta})\#p_{n-1}\|q) + \frac{1}{2\gamma} \mathbb{E}_{x \sim p_{n-1}} \|x - F_{n,\theta}(x)\|^2. \quad (22)$$

When $q = \mathcal{N}(0, I)$, we have $V(x) = \|x\|^2/2$. Then, by the instantaneous change-of-variable formula (13), the KL divergence term in (22) expands to

$$\text{KL}((F_{n,\theta})\#p_{n-1}\|q) = \mathbb{E}_{x(t_{n-1}) \sim p_{n-1}} \left(\frac{x(t_n)^2}{2} - \int_{t_{n-1}}^{t_n} \nabla \cdot v_{\theta}(x(\tau), \tau) d\tau \right) + \text{const.} \quad (23)$$

Example: JKO flow as pushforwarding particles. The minimization of (the empirical version of) (22)(23) in each step of the JKO flow is ready to be computed on particles $\{x^i\}_{i=1}^m$, namely the finite data samples. To illustrate such an iteration, consider an example with $m = 3$ particles, as shown in Fig. 6. Initially, at $t_0 = 0$, the particle positions correspond to training samples $x^i(0) = x^i$. In the first iteration, we train the first residual block, and the velocity field $v_{\theta}(x, t)$ over the interval $t \in [t_0, t_1]$ is modeled by a neural network with parameters θ . The empirical version of (22)(23) gives the training objective of the first block as

$$\min_{\theta} \frac{1}{m} \sum_{i=1}^m \left(\frac{x^i(t_1)^2}{2} - \int_{t_0}^{t_1} \nabla \cdot v_{\theta}(x^i(\tau; \theta), \tau) d\tau \right) + \frac{1}{2\gamma m} \sum_{i=1}^m \|x^i(t_1) - x^i(t_0)\|^2, \quad (24)$$

where $\gamma > 0$ controls the step size. After the first block is trained, the particle positions are updated using the learned transport map (14) on $[t_0, t_1]$, namely,

$$x^i(t_1) = x^i(t_0) + \int_{t_0}^{t_1} v_{\theta}(x^i(t), t) dt, \quad \dot{x}^i(t) = v_{\theta}(x^i(t), t), \quad x^i(t_0) = x^i.$$

In the next iteration, we train the velocity field $v_{\theta}(x, t)$ over the time interval $[t_1, t_2]$, and the initial positions of the particles are $x^i(t_1)$ which have been computed from the previous iteration. This

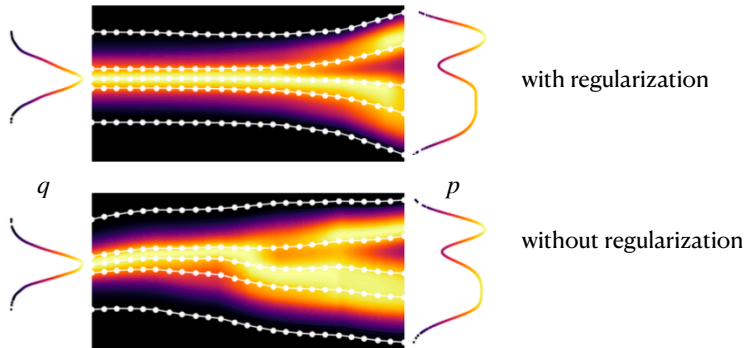


Figure 7: Trajectory of flow between p and q with and without regularization: Regularization results in “straighter paths” for the particles, requiring fewer steps to transition from p to q and reducing the number of neural network blocks in the implementation.

procedure continues for $n = 1, 2, \dots, N$ for N steps (Residual blocks).

4.2 Interpretation of Wasserstein regularization term

Before imposing the flow network parametrization, the original JKO scheme (19) can be interpreted as the \mathcal{W}_2 -proximal Gradient Descent (GD) of the KL objective [32, 8] with step size controlled by γ . This naturally provides a variational interpretation of the iterative flow model as implementing a discrete-time GD on the \mathcal{W}_2 space. The connection to Wasserstein GD allows us to prove the generation guarantee of such flow models by analyzing the convergence of proximal GD in Wasserstein space, to be detailed in Section 4.4.

Meanwhile, the per-step training objective (21) can be viewed as the addition of the variational objective (closeness of the pushforwarded density to target q) and the Wasserstein term (the squared \mathcal{W}_2 distance between the pushforwarded density and the current density). The Wasserstein term serves to *regularize* the “amount of movement” from the current density p_{n-1} by the transport map $F_{n,\theta}$. Intuitively, among all transports $F_{n,\theta}$ that can successfully reduce the KL divergence from $(F_{n,\theta})\#p_{n-1}$ to q , the regularization term will select the one that has the smallest movement. By limiting excessive movement from one iteration to the next, the \mathcal{W}_2 regularization term leads to straighter transport paths in probability space, as illustrated in Fig. 7. It may also reduce the number of neural network blocks needed to reach the target distribution. In a particle-based implementation of the n -th flow block, this \mathcal{W}_2 term can be computed as $\frac{1}{m} \sum_{i=1}^m \|x^i(t_n) - x^i(t_{n-1})\|^2$, the average squared movement over m particles, making use of the ODE trajectories $x^i(t)$.

4.3 Simulation-free iterative flow via local Flow Matching

The per-step training in Section 4.1 is based on likelihood (KL divergence) and not simulation-free. It would be desirable to incorporate simulation-free training, such as Flow Matching (FM), under the iterative flow framework. To this end, [39] developed Local Flow Matching by introducing an

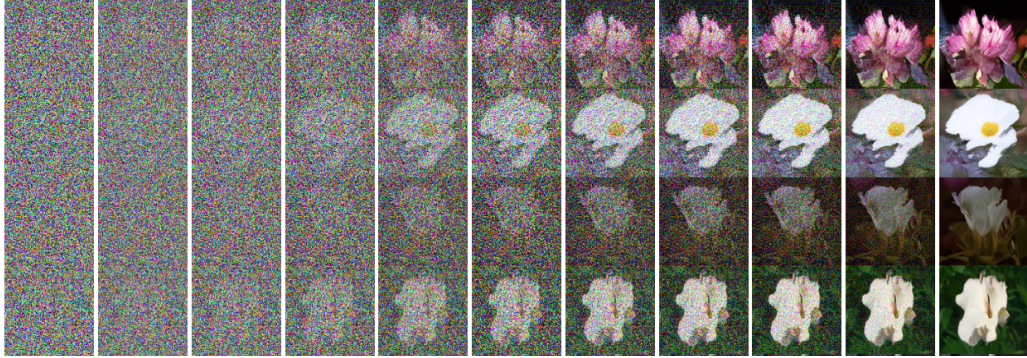


Figure 8: Noise-to-image trajectories of Flowers data by Local Flow Matching [39].

iterative, block-wise training approach, where each step implements a simulation-free training of an FM objective. The previous (global) FM model directly interpolates between noise and data distributions, which may differ significantly. In contrast, Local FM decomposes this transport into smaller, incremental steps, interpolating between distributions that are closer to each other, hence the name “local.” The Local FM model trains a sequence of small, invertible sub-flow models, which, when concatenated, transform between the data and noise distributions; a real data example is shown in Fig. 8.

4.4 Theoretical analysis of generation guarantee

Most theoretical results on deep generative models focus on score-based diffusion models (the forward process is always an SDE), e.g. the latest ones like [7, 23], and (end-to-end training, global) flow models (in both forward and reverse processes) such as recent works: for the flow-matching model [5] and applied to probability flow ODE in score-based diffusion models; for neural ODE models trained by likelihood maximization (the framework in [14]) [26].

Below, we highlight a key insight in analyzing iterative flow models by making the connection to the convergence of Wasserstein GD. Because the Wasserstein GD will be shown to have linear (exponential) convergence, such analysis bounds the needed number of iterative steps N (number of Residual blocks) to be $\sim \log(1/\varepsilon)$ for the flow model to achieve an $O(\varepsilon)$ amount of “generation error”, which is measured by the divergence between the generated distribution and the true data distribution. Here we follow the proof for the JKO flow model [8], and similar idea has been applied to prove the convergence of Local FM [39].

To study the evolution of probability densities, we adopt the Wasserstein space as the natural setting, as it captures the geometric structure of probability distributions via transport maps. Recall the iterative scheme in Section 4.1 produces a sequence of distributions in the \mathcal{W}_2 space from data

to noise and back, which we denote as the *forward process* and the *reverse process* respectively:

$$\begin{aligned}
 \text{(forward)} \quad p &= p_0 \xrightarrow{F_1} p_1 \xrightarrow{F_2} \dots \xrightarrow{F_N} p_N \approx q, \\
 \text{(reverse)} \quad p &\approx q_0 \xleftarrow{F_1^{-1}} q_1 \xleftarrow{F_2^{-1}} \dots \xleftarrow{F_N^{-1}} q_N = q,
 \end{aligned} \tag{25}$$

The density q_0 is the generated density by the learned flow model, and the goal is to show that q_0 is close to data density $p = p_0$. The proof framework consists of establishing convergence guarantees first for the forward process and consequently for the reverse process:

Forward process (data-to-noise) convergence.

- At each iteration of minimizing (21) which gives a pushforwarded p_n by the learned $F_{n,\theta}$, we assume that the minimization is approximately solved with the amount of error $O(\varepsilon)$ that is properly defined.
- The forward convergence guarantee is by mirroring the analysis of vector space (proximal) GD for convex optimization analysis. Specifically, making use of the λ -convexity of $G(\rho) := \text{KL}(\rho||q)$ in Wasserstein space, one can show the Evolution Variational Inequality (EVI):

$$\left(1 + \frac{\gamma\lambda}{2}\right) \mathcal{W}^2(p_{n+1}, q) + 2\gamma (G(p_{n+1}) - G(q)) \leq \mathcal{W}^2(p_n, q) + O(\varepsilon^2).$$

- The EVI is a key step to establish the exponential convergence of the Wasserstein GD and the guarantee of closeness between p_n to q in KL-divergence. Specifically, $O(\varepsilon^2)$ KL-divergence is obtained after approximately $\log(1/\varepsilon)$ JKO steps (Residual blocks).

Reverse process (noise-to-data) convergence. The convergence of the reverse process follows by the invertibility of the flow map, and we utilize the following key lemma, Bi-direction Data Processing Inequality (DPI) for f -divergences. Let p and q be two probability distribution, such that p is absolutely continuous with respect to q . For a convex function $f : [0, \infty) \rightarrow \mathbb{R}$ such that f is finite for all $x > 0$, $f(1) = 0$, and f is right-continuous at 0, the f -divergence of p from q is defined as $D_f(p||q) = \int f\left(\frac{p(x)}{q(x)}\right) q(x)dx$; for instance, KL-divergence is an f -divergence.

Lemma 4.1 (Bi-direction DPI). *Let D_f be an f -divergence. If $F : \mathbb{R}^d \rightarrow \mathbb{R}^d$ is invertible and for two densities p and q on \mathbb{R}^d , $F_{\#}p$ and $F_{\#}q$ also have densities, then*

$$D_f(p||q) = D_f(F_{\#}p||F_{\#}q).$$

The proof is standard and can be found in [39, 29]. The DPI controls information loss in both forward and reverse transformations. Bringing these results together provides a density learning guarantee. Because KL-divergence is an f -divergence, the closeness at the end of the forward process in terms of $\text{KL}(p_N||q_N = q)$ directly implies the same closeness at the end of the reverse process, i.e. $\text{KL}(p_0 = p||q_0)$; see (25). The $O(\varepsilon^2)$ KL control implies $O(\varepsilon)$ bound in Total Variation.

5 Applications and extensions

In this section, we present various applications and extensions of the previously discussed flow-based generative models to problems in statistics, signal processing, and machine learning, involving a general target density and a general loss function.

5.1 Data synthesis and evaluation metrics

Synthetic data generation is a common application of generative models, aiming to learn complex data distributions of the training data and synthesize new data samples that follow the same distribution. In image generation, generative models effectively capture intricate patterns, textures, and structures from large datasets, enabling them to generate high-quality images that closely resemble real-world data. This capability has numerous applications in computer vision, content creation, and medical imaging, where synthetic images can enhance training datasets and enable downstream machine learning tasks.

For data synthesis tasks, generative models are evaluated using various metrics that assess the quality, diversity, and likelihood of the generated samples. Commonly used metrics include Fréchet Inception Distance (FID), Negative Log-Likelihood (NLL), KL Divergence, Log-Likelihood per Dimension, Precision and Recall for Distributions, Inception Score (IS), and Perceptual Path Length (PPL). Other metrics for comparing two sets of sample distributions can also be used to evaluate generation quality, such as the kernel Maximum Mean Discrepancy (MMD) statistic. Among these, FID and NLL are the most frequently used for assessing both perceptual quality and likelihood estimation in flow-based models. In practice, researchers often report both FID and NLL when evaluating flow-based generative models.

FID is a widely used metric that measures the distance between the feature distributions of real and generated images. It is computed as the Fréchet distance between two multivariate Gaussian distributions, one representing real images and the other representing generated images. Mathematically, FID is given by: $\|\mu_r - \mu_g\|^2 + \text{Tr}(\Sigma_r + \Sigma_g - 2(\Sigma_r \Sigma_g)^{1/2})$ where μ_r, Σ_r are the mean and covariance matrix of data in feature space, and μ_g, Σ_g are the mean and covariance matrix of generated data. The first term captures differences in mean, while the second term accounts for differences in variance. Lower FID values indicate better sample quality and diversity. FID provides an empirical assessment of whether the generated samples match the real data distribution in a perceptual feature space, which is important in applications where sample quality is crucial, such as image generation.

Negative Log-Likelihood (NLL) is a direct measure of how well a generative model fits the training data distribution. Given a test dataset $\{\tilde{x}^i\}_{i=1}^{m'}$ and a model (e.g., learned by flow model) with probability density function $p_\theta(x)$, the NLL is computed as: $\text{NLL} = -\frac{1}{m'} \sum_{i=1}^{m'} \log p_\theta(\tilde{x}^i)$ where $p_\theta(x)$ is the model's probability density at test sample \tilde{x}^i . Lower NLL values indicate that the model assigns high probability to real data, meaning it has effectively captured the distribution. Conversely, higher NLL values suggest poor data fit. Since flow-based models explicitly learn

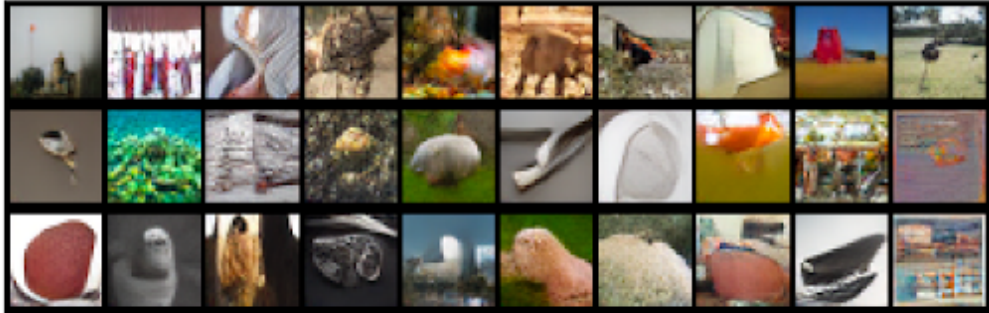


Figure 9: Example of JKO-flow generated synthetic images (with FID 20.1), trained using ImageNet-32 dataset with 1,281,167 training samples. Labels identified for the first 10 images (first row) by a classification algorithm are 1: ‘flagpole’, 2: ‘ski’, 3: ‘Windsor tie’, 4: ‘Gila monster’, 5: ‘goldfish’, 6: ‘warthog’, 7: ‘admiral’, 8: ‘envelope’, 9: ‘barn’, 10: ‘ostrich’.

the data distribution, NLL serves as a fundamental evaluation metric, complementing perceptual metrics like FID, but it does not always correlate with perceptual sample quality. Fig. 2 illustrated NLL scores for various generative models.

5.2 General q rather than Gaussian

In many applications, the goal is to learn a mapping from p to a general distribution q rather than restricting q to a Gaussian. For instance, in image applications, generative models can interpolate between different styles, manipulate image attributes, and generate high-resolution outputs, making them powerful tools for various real-world tasks. This has significant implications for transfer learning, domain adaptation, and counterfactual analysis. In a broader sense, this task aligns with the Schrödinger bridge problem, which seeks stochastic processes that interpolate between given marginal distributions. A flow-based approach provides a generalizable framework for addressing this problem [40].

Flow-based Optimal Transport. The formulation is based on the idea of finding the optimal transport map between two distributions. The celebrated Benamou-Brenier equation expresses Optimal Transport (OT) in a dynamic setting [36, 4]:

$$\begin{aligned} \mathcal{T} &:= \inf_{\rho, v} \int_0^1 \mathbb{E}_{x(t) \sim \rho(\cdot, t)} \|v(x(t), t)\|^2 dt \\ \text{s.t. } &\partial_t \rho + \nabla \cdot (\rho v) = 0, \quad \rho(\cdot, 0) = p, \quad \rho(\cdot, 1) = q, \end{aligned} \tag{26}$$

where $v(x, t)$ represents the velocity field, and $\rho(x, t)$ is the probability density at time t , evolving according to the CE. Under suitable regularity conditions, the minimum transport cost \mathcal{T} in (26) equals the squared Wasserstein-2 distance, and the optimal velocity field $v(x, t)$ provides a control function for the transport process.

Motivated by this, we solve the OT problem by introducing a regularized optimization formu-

lation:

$$\int_0^1 \mathbb{E}_{x(t) \sim \rho(t)} \|v(x(t), t)\|_2^2 dt + \frac{1}{2\gamma} \text{KL}(p \|\hat{p}) + \frac{1}{2\gamma} \text{KL}(q \|\hat{q}), \quad (27)$$

where $\gamma > 0$ is a regularization parameter enforcing terminal constraints through KL divergence terms, and \hat{p} and \hat{q} denote the transported distributions obtained via the learned velocity field using CE. The symmetry and invertibility of the transport map allow us to impose constraints on both forward and reverse mappings. A particle-based approach can approximate the discrete-time transport cost; for instance, over a segment $[t_0, t_1]$:

$$\int_{t_0}^{t_1} \mathbb{E}_{x(t) \sim \rho_t} \|v(x(t), t)\|_2^2 dt \approx \frac{1}{(t_1 - t_0)m} \sum_{i=1}^m \|x^i(t_1) - x^i(t_0)\|_2^2.$$

Finally, the KL divergence terms can be estimated from particles at the two endpoints by estimating the log-likelihood function $\log q(x)/p(x)$, which can be estimated using a technique training a classification network, based on Lemma 5.1 below.

Estimating density ratios via learned velocity fields. The velocity field learned from (27) can also be used for density ratio estimation (DRE), a fundamental problem in statistics and machine learning with applications in hypothesis testing, change-point detection, anomaly detection, and mutual information estimation. A major challenge in DRE arises when the supports of p and q differ significantly. To mitigate this, one technique is the telescopic density ratio estimation [30, 9], which introduces intermediate distributions that bridge between p and q : Given a sequence of intermediate densities p_n for $k = 0, \dots, N$ with $p_0 = p$ and $p_N = q$, consecutive pairs (p_n, p_{n+1}) are chosen such that their supports are close to facilitate accurate density ratio estimation. The log-density ratio can then be computed via a telescopic series as:

$$\log \frac{q(x)}{p(x)} = \log p_N(x) - \log p_0(x) = \sum_{n=0}^{N-1} (\log p_{n+1}(x) - \log p_n(x)). \quad (28)$$

This multi-step approach improves estimation accuracy compared to direct one-step DRE.

Using flow-based neural networks, we can learn the velocity field that transports particles between intermediate distributions and estimate density ratios at each step—for instance, by leveraging classification-based networks to distinguish between samples at consecutive time steps. The classification-based network can lead to an estimate for the log-likelihood between two distributions (using their samples) due to the following lemma that is straightforward to verify (see, e.g., [22]):

Lemma 5.1 (Training of logistic loss leads to KL divergence under population loss and perfect training). *For logistic loss, given two distributions f_0 and f_1 , let*

$$\ell[\varphi] = \int \log(1 + e^{\varphi(x)}) f_0(x) dx + \int \log(1 + e^{-\varphi(x)}) f_1(x) dx,$$

Then the functional global minimizer is given by $\varphi^ = \log(f_1/f_0)$.*

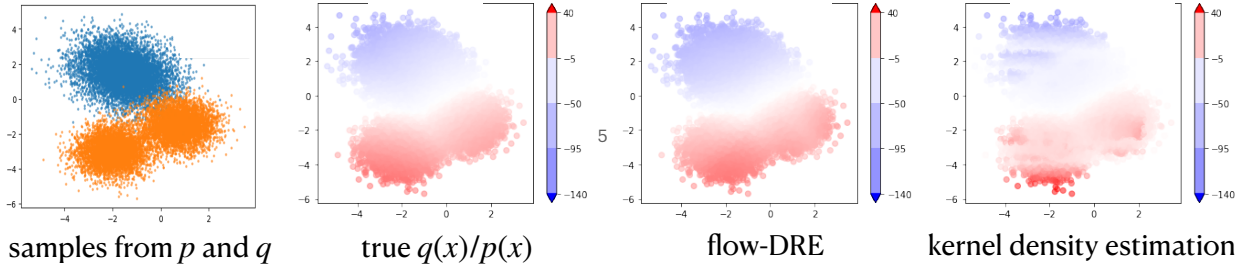


Figure 10: Density ratio between two Gaussian mixtures with very different support: $p = \frac{1}{3}\mathcal{N}([-2, 2]^T, 0.75I_2) + \frac{1}{3}\mathcal{N}([-1.5, 1.5]^T, 0.25I_2) + \frac{1}{3}\mathcal{N}([-1, 1]^T, 0.75I_2)$ and $q = \frac{1}{2}\mathcal{N}([0.75, -1.5]^T, 0.5I_2) + \frac{1}{2}\mathcal{N}([-2, -3]^T, 0.5I_2)$, obtained via flow-based density ratio estimation, which provides a more accurate approximation of the true density ratio compared to standard kernel density estimation (KDE). A similar example was used in [40]; here we further compare with KDE.



Figure 11: Illustrative examples of images generated by the adversarial sampler by solving (29); note that after the “worsening” transformation, the image becomes misclassified.

An illustrative example is shown in Fig. 10. We remark that although this telescopic density ratio learning scheme, in principle, works with an arbitrary velocity field, an “optimal” velocity field (e.g., one that minimizes the “energy”) tends to be more efficient in implementation and achieves better numerical accuracy.

5.3 Sampling from worst-case distribution

The proposed framework can be used beyond finding distributions that match the original data distribution, but also find the worst-case distributions in distributional robust optimization (DRO) problem (see, e.g., a survey [21]) with application to robust learning. In this setting, the target distribution q is not pre-specified but is instead induced by a problem-specific risk function $R(\cdot) : \mathbb{R}^d \rightarrow \mathbb{R}$. The formulation is based on the following so-called flow-based DRO problem [41], where the objective is to solve a transport map:

$$\min_F \mathbb{E}_{X \sim p} [R(F(X)) + \frac{1}{2\gamma} \|X - F(X)\|_2^2]. \quad (29)$$

for a given regularization parameter $\gamma > 0$. Here, the reference measure p can be represented by a pre-trained generative model. Thus, this framework allows to adapt the pre-trained generative model from synthesize samples that follows the same distribution as the training data, to produce the worst-case samples that maximize the risk function R – representing the unseen scenarios. Using a flow-based model to represent transport map F , the above optimization problem can be solved by the aforementioned framework. The learned transformation F^* defines the worst-case sampler, inducing the adversarial distribution $q = F^*_{\#}p$, which transforms generated samples to regions that lead to higher risk. As an example, Figure 11 illustrates an adversarial sampler for classification algorithms, where the risk function R is chosen as the classification accuracy (cross-entropy loss). In this case, the generated images are mapped to cause misclassification, demonstrating how the framework can be used to generate adversarial samples from worst-case distributions in practical applications.

6 Conclusion

Flow-based generative models represent a compelling framework for high-dimensional probability modeling, offering advantages such as exact likelihood computation, invertible transformations, and efficient sample generation. By leveraging ODEs and optimal transport techniques, flow-based models provide a general framework for density estimation and data synthesis, making them particularly well-suited for signal processing applications. In this tutorial, we presented a mathematical and algorithmic perspective on flow-based generative models, introducing key concepts such as continuous normalizing flows (CNFs), Flow Matching (FM), and iterative training via the Jordan-Kinderlehrer-Otto (JKO) scheme. Through the lens of Wasserstein gradient flows, we demonstrated how these models naturally evolve within probability space, offering both theoretical guarantees and practical scalability. Additionally, we explored extensions of flow-based models, including generalization beyond Gaussian target distributions and to include general loss for worst-case sampling via distributionally robust optimization (DRO).

There are many areas we did not cover in this tutorial. Notably, flow-based generative models can be extended for conditional generation, where the model generates data given some condition, such as class labels, textual descriptions, or auxiliary variables. This has applications in network-based conditional generation [37]. Flow model can also be utilized for sampling posterior (see, e.g., [28]). Additionally, counterfactual sampling is another promising direction, allowing for the generation of synthetic samples that were not observed in real-world data but could have occurred under different causal assumptions.

By providing both theoretical insights and practical guidelines, this tutorial aims to equip researchers and practitioners with the necessary tools to develop and apply flow-based generative models in diverse domains. As these models continue to evolve, their integration with advanced optimization and machine learning techniques will further expand their impact on modern signal processing, statistical inference, and generative AI applications.

Acknowledgment

This work is partially supported by NSF DMS-2134037. YX is also partially supported by the Coca-Cola Foundation. XC is also partially supported by NSF DMS-2237842 and Simons Foundation (grant ID: MPS-MODL-00814643). The authors thank Chen Xu for help with numerical examples.

References

- [1] Michael S Albergo and Eric Vanden-Eijnden. Building normalizing flows with stochastic interpolants. In *ICLR*, 2023.
- [2] David Alvarez-Melis, Yair Schiff, and Youssef Mroueh. Optimizing functionals on the space of probabilities with input convex neural networks. *Transactions on Machine Learning Research*, 2022.
- [3] Luigi Ambrosio, Nicola Gigli, and Giuseppe Savaré. *Gradient flows: In metric spaces and in the space of probability measures*. Springer Science & Business Media, 2005.
- [4] Jean-David Benamou and Yann Brenier. A computational fluid mechanics solution to the monge-kantorovich mass transfer problem. *Numerische Mathematik*, 84(3):375–393, 2000.
- [5] J Benton, G Deligiannidis, and A Doucet. Error bounds for flow matching methods. *Transactions on Machine Learning Research*, 2024.
- [6] Ricky TQ Chen, Yulia Rubanova, Jesse Bettencourt, and David K Duvenaud. Neural ordinary differential equations. *NeurIPS*, 31, 2018.
- [7] Sitan Chen, Sinho Chewi, Holden Lee, Yuanzhi Li, Jianfeng Lu, and Adil Salim. The probability flow ODE is provably fast. *NeurIPS*, 36, 2024.
- [8] Xiuyuan Cheng, Jianfeng Lu, Yixin Tan, and Yao Xie. Convergence of flow-based generative models via proximal gradient descent in Wasserstein space. *IEEE Transactions on Information Theory*, 2024.
- [9] Kristy Choi, Chenlin Meng, Yang Song, and Stefano Ermon. Density ratio estimation via infinitesimal classification. In *International Conference on Artificial Intelligence and Statistics*, pages 2552–2573. PMLR, 2022.
- [10] Laurent Dinh, David Krueger, and Yoshua Bengio. NICE: Non-linear independent components estimation. *International Conference on Learning Representations (ICLR) Workshop*, 2015.
- [11] Laurent Dinh, Jascha Sohl-Dickstein, and Samy Bengio. Density estimation using Real NVP. In *International Conference on Learning Representations (ICLR)*, 2017.

- [12] Patrick Esser, Sumith Kulal, Andreas Blattmann, Rahim Entezari, Jonas Müller, Harry Saini, Yam Levi, Dominik Lorenz, Axel Sauer, Frederic Boesel, et al. Scaling rectified flow transformers for high-resolution image synthesis. In *ICML*, 2024.
- [13] Jiaojiao Fan, Qinsheng Zhang, Amirhossein Taghvaei, and Yongxin Chen. Variational Wasserstein gradient flow. In *ICML*, pages 6185–6215. PMLR, 2022.
- [14] Will Grathwohl, Ricky TQ Chen, Jesse Bettencourt, Ilya Sutskever, and David Duvenaud. FFJORD: Free-form continuous dynamics for scalable reversible generative models. In *ICLR*, 2018.
- [15] Wenhao Guan, Kaidi Wang, Wangjin Zhou, Yang Wang, Feng Deng, Hui Wang, Lin Li, Qingyang Hong, and Yong Qin. LAFMA: A latent flow matching model for text-to-audio generation. In *Interspeech 2024*, Kos, Greece, 2024.
- [16] Kaiming He, Xiangyu Zhang, Shaoqing Ren, and Jian Sun. Deep residual learning for image recognition. In *Proceedings of the IEEE conference on computer vision and pattern recognition*, pages 770–778, 2016.
- [17] Jonathan Ho, Ajay Jain, and Pieter Abbeel. Denoising diffusion probabilistic models. *NeurIPS*, 33:6840–6851, 2020.
- [18] Richard Jordan, David Kinderlehrer, and Felix Otto. The variational formulation of the fokker–planck equation. *SIAM journal on mathematical analysis*, 29(1):1–17, 1998.
- [19] Durk P Kingma and Prafulla Dhariwal. Glow: Generative flow with invertible 1x1 convolutions. *Advances in neural information processing systems*, 31, 2018.
- [20] Ivan Kobyzev, Simon JD Prince, and Marcus A Brubaker. Normalizing flows: An introduction and review of current methods. *IEEE Transactions on Pattern Analysis and Machine Intelligence*, 43(11):3964–3979, 2020.
- [21] Daniel Kuhn, Peyman Mohajerin Esfahani, Viet Anh Nguyen, and Soroosh Shafieezadeh-Abadeh. Wasserstein distributionally robust optimization: Theory and applications in machine learning. In *Operations research & management science in the age of analytics*, pages 130–166. Informs, 2019.
- [22] Junghwan Lee, Yao Xie, and Xiuyuan Cheng. Training neural networks for sequential change-point detection. In *ICASSP 2023-2023 IEEE International Conference on Acoustics, Speech and Signal Processing (ICASSP)*, pages 1–5. IEEE, 2023.
- [23] Gen Li, Yuting Wei, Yuxin Chen, and Yuejie Chi. Towards non-asymptotic convergence for diffusion-based generative models. In *ICLR*, 2024.
- [24] Yaron Lipman, Ricky T. Q. Chen, Heli Ben-Hamu, Maximilian Nickel, and Matthew Le. Flow matching for generative modeling. In *ICLR*, 2023.

- [25] Qiang Liu. Rectified flow: A marginal preserving approach to optimal transport. *arXiv:2209.14577*, 2022.
- [26] Youssef Marzouk, Zhi Ren, Sven Wang, and Jakob Zech. Distribution learning via neural differential equations: a nonparametric statistical perspective. *Journal of Machine Learning Research*, 2024.
- [27] Petr Mokrov, Alexander Korotin, Lingxiao Li, Aude Genevay, Justin M Solomon, and Evgeny Burnaev. Large-scale Wasserstein gradient flows. *NeurIPS*, 34:15243–15256, 2021.
- [28] Vishal Purohit, Matthew Repasky, Jianfeng Lu, Qiang Qiu, Yao Xie, and Xiuyuan Cheng. Posterior sampling via langevin dynamics based on generative priors. *arXiv preprint arXiv:2410.02078*, 2024.
- [29] Maxim Raginsky. Strong data processing inequalities and Φ -Sobolev inequalities for discrete channels. *IEEE Transactions on Information Theory*, 62(6):3355–3389, 2016.
- [30] Benjamin Rhodes, Kai Xu, and Michael U. Gutmann. Telescoping density-ratio estimation. In H. Larochelle, M. Ranzato, R. Hadsell, M.F. Balcan, and H. Lin, editors, *Advances in Neural Information Processing Systems*, volume 33, pages 4905–4916. Curran Associates, Inc., 2020.
- [31] Quentin Rouxel, Andrea Ferrari, Serena Ivaldi, and Jean-Baptiste Mouret. Flow matching imitation learning for multi-support manipulation. In *2024 IEEE-RAS 23rd International Conference on Humanoid Robots (Humanoids)*, pages 528–535. IEEE, 2024.
- [32] Adil Salim, Anna Korba, and Giulia Luise. The wasserstein proximal gradient algorithm. *Advances in Neural Information Processing Systems*, 33:12356–12366, 2020.
- [33] Yang Song, Jascha Sohl-Dickstein, Diederik P Kingma, Abhishek Kumar, Stefano Ermon, and Ben Poole. Score-based generative modeling through stochastic differential equations. In *International Conference on Learning Representations (ICLR)*, 2021.
- [34] Yang Song, Jascha Sohl-Dickstein, Diederik P Kingma, Abhishek Kumar, Stefano Ermon, and Ben Poole. Score-based generative modeling through stochastic differential equations. In *ICLR*, 2021.
- [35] Alexander Vidal, Samy Wu Fung, Luis Tenorio, Stanley Osher, and Levon Nurbekyan. Taming hyperparameter tuning in continuous normalizing flows using the JKO scheme. *Scientific Reports*, 13(1):4501, 2023.
- [36] Cédric Villani et al. *Optimal Transport: Old and New*. Springer, 2009.
- [37] Chen Xu, Xiuyuan Cheng, and Yao Xie. Invertible neural networks for graph prediction. *IEEE Journal on Selected Areas in Information Theory*, 3(3):454–467, 2022.

- [38] Chen Xu, Xiuyuan Cheng, and Yao Xie. Normalizing flow neural networks by JKO scheme. *Conference on Neural Information Processing Systems (NeurIPS)*, 2023.
- [39] Chen Xu, Xiuyuan Cheng, and Yao Xie. Local flow matching generative models. *arXiv preprint arXiv:2410.02548*, 2024.
- [40] Chen Xu, Xiuyuan Cheng, and Yao Xie. Computing high-dimensional optimal transport by flow neural networks. *International Conference on Artificial Intelligence and Statistics (AISTATS)*, 2025.
- [41] Chen Xu, Jonghyeok Lee, Xiuyuan Cheng, and Yao Xie. Flow-based distributionally robust optimization. *IEEE Journal on Selected Areas in Information Theory*, 2024.

A Proof of Lemma 3.1

The same result was proved in [1, Proposition 1] where it was assumed that x_0 and x_1 are independent. Here, we show that allowing dependence between x_0 and x_1 does not harm the conclusion.

Proof of Lemma 3.1. We denote the joint density of x_0, x_1 as $\rho_{0,1}(x_0, x_1)$, and it satisfies that the two marginals are p and q respectively. We denote $v(\cdot, t)$ as $v_t(\cdot)$ and $\rho(\cdot, t)$ as $\rho_t(\cdot)$. We will first explicitly construct ρ_t and v_t , and then show that ρ_t indeed solves the CE induced by v_t , and that v_t is valid.

Let $\rho_t(x)$ be the concentration of the interpolant points $I_t(x_0, x_1)$ over all possible realizations of the two endpoints, that is, using a formal derivation with the Dirac delta measure δ (the mathematical derivation using Fourier representation and under technical conditions can be found in [1, Lemma B.1]), we define

$$\rho_t(x) := \int_{\mathbb{R}^d} \int_{\mathbb{R}^d} \delta(x - I_t(x_0, x_1)) \rho_{0,1}(x_0, x_1) dx_0 dx_1.$$

Because $I_0(x_0, x_1) = x_0$ and $I_1(x_0, x_1) = x_1$, we know that

$$\rho_0(x) = \int \rho_{0,1}(x, x_1) dx_1 = p(x), \quad \rho_1(x) = \int \rho_{0,1}(x_0, x) dx_0 = q(x).$$

By definition,

$$\partial_t \rho_t(x) = - \int_{\mathbb{R}^d} \int_{\mathbb{R}^d} \partial_t I_t(x_0, x_1) \cdot \nabla \delta(x - I_t(x_0, x_1)) \rho_{0,1}(x_0, x_1) dx_0 dx_1 = -\nabla \cdot j_t(x), \quad (30)$$

where

$$j_t(x) := \int_{\mathbb{R}^d} \int_{\mathbb{R}^d} \partial_t I_t(x_0, x_1) \delta(x - I_t(x_0, x_1)) \rho_{0,1}(x_0, x_1) dx_0 dx_1.$$

We now define v_t to be such that

$$v_t(x) \rho_t(x) = j_t(x),$$

this can be done by setting $v_t(x) = j_t(x)/\rho_t(x)$ if $\rho_t(x) > 0$ and zero otherwise. Then, (30) directly gives that $\partial_t \rho_t = -\nabla \cdot (\rho_t v_t)$ which is the CE. This means that v_t is a valid velocity field.

To prove the lemma, it remains to show that the loss (16) can be equivalently written as (17). To see this, note that (16) can be written as

$$L(\hat{v}) = \int_0^1 l(\hat{v}, t) dt, \quad l(\hat{v}, t) := \mathbb{E}_{x_0, x_1} \|\hat{v}_t(I_t(x_0, x_1)) - \partial_t I_t(x_0, x_1)\|^2. \quad (31)$$

For a fixed t ,

$$\begin{aligned} l(\hat{v}, t) &= \int_{\mathbb{R}^d} \int_{\mathbb{R}^d} \|\hat{v}_t(I_t(x_0, x_1)) - \partial_t I_t(x_0, x_1)\|^2 \rho_{0,1}(x_0, x_1) dx_0 dx_1 \\ &= \int_{\mathbb{R}^d} \int_{\mathbb{R}^d} \int_{\mathbb{R}^d} \|\hat{v}_t(x) - \partial_t I_t(x_0, x_1)\|^2 \delta(x - I_t(x_0, x_1)) \rho_{0,1}(x_0, x_1) dx_0 dx_1 dx \\ &= c_1(t) + \int_{\mathbb{R}^d} \int_{\mathbb{R}^d} \int_{\mathbb{R}^d} (\|\hat{v}_t(x)\|^2 - 2\hat{v}_t(x) \cdot \partial_t I_t(x_0, x_1)) \delta(x - I_t(x_0, x_1)) \rho_{0,1}(x_0, x_1) dx_0 dx_1 dx, \end{aligned}$$

where

$$c_1(t) := \int_{\mathbb{R}^d} \int_{\mathbb{R}^d} \|\partial_t I_t(x_0, x_1)\|^2 \rho_{0,1}(x_0, x_1) dx_0 dx_1,$$

and $c_1(t)$ is independent from \hat{v} . We continue the derivation as

$$\begin{aligned} l(\hat{v}, t) - c_1(t) &= \int_{\mathbb{R}^d} \|\hat{v}_t(x)\|^2 \int_{\mathbb{R}^d} \int_{\mathbb{R}^d} \delta(x - I_t(x_0, x_1)) \rho_{0,1}(x_0, x_1) dx_0 dx_1 dx \\ &\quad - 2 \int_{\mathbb{R}^d} \hat{v}_t(x) \cdot \int_{\mathbb{R}^d} \int_{\mathbb{R}^d} \partial_t I_t(x_0, x_1) \delta(x - I_t(x_0, x_1)) \rho_{0,1}(x_0, x_1) dx_0 dx_1 dx \\ &= \int_{\mathbb{R}^d} \|\hat{v}_t(x)\|^2 \rho_t(x) dx - 2 \int_{\mathbb{R}^d} \hat{v}_t(x) \cdot j_t(x) dx \\ &= \int_{\mathbb{R}^d} (\|\hat{v}_t(x)\|^2 - 2\hat{v}_t(x) \cdot v_t(x)) \rho_t(x) dx \\ &= \int_{\mathbb{R}^d} \|\hat{v}_t(x) - v_t(x)\|^2 \rho_t(x) dx - \int_{\mathbb{R}^d} \|v_t(x)\|^2 \rho_t(x) dx, \end{aligned}$$

and then, by defining

$$c_2(t) := \int_{\mathbb{R}^d} \|v_t(x)\|^2 \rho_t(x) dx,$$

which is again independent from \hat{v} , we have

$$l(\hat{v}, t) = \int_{\mathbb{R}^d} \|\hat{v}_t(x) - v_t(x)\|^2 \rho_t(x) dx + c_1(t) - c_2(t).$$

Putting back to (31) we have proved the lemma, where the constant $c = \int_0^1 (c_1(t) - c_2(t)) dt$. \square